Lantana camara Mediated Synthesis of Gold Nanoparticles: Exploration of their Antibacterial and Anticancer Potentials in Oral Cancer Therapy

Xiaoqiang Wu *

Oral cancer is the sixth most prevalent malignancy worldwide. Gold nanoparticles (AuNPs) were prepared using *Lantana camara* leaf extract and evaluate their *in vitro* anticancer activity against human KB cells. The AuNPs were characterized using various techniques. The MTT assay was employed to evaluate the cytotoxic potential of AuNPs against KB cells. Staining techniques were used to quantify reactive oxygen species (ROS) levels and assess apoptotic cell death in AuNP-treated KB cells. Furthermore, the caspase activities were examined to verify the induction of apoptosis. The antibacterial activity of AuNPs was also evaluated against gram-negative and gram-positive bacterial strains. The results indicated that the synthesized AuNPs exhibited predominantly spherical morphology with an average particle size of 40 to 80 nm. The assay revealed a dose-dependent cytotoxic effect, with an IC_{50} value of 30 µg/mL against KB cells formulated AuNPs effectively inhibited KB cell proliferation, enhanced intracellular ROS generation, and induced apoptosis, as confirmed by fluorescence staining and elevated caspase activities. The AuNPs demonstrated significant antibacterial properties, producing inhibition zones of up to 23 mm against *Staphylococcus aureus* and 15 mm against *Escherichia coli.* In summary, the *L. camara*-mediated AuNPs exhibited a substantial anticancer potential against oral cancer cells and demonstrated encouraging antibacterial properties.

DOI: 10.15376/biores.21.4.10205-10223

Keywords: Gold nanoparticles; Lantana camara; Oral cancer; Cytotoxicity; ROS; Caspases; Anti-microbial

Contact information: Department of Nursing, Wulanchabu Medical College, Ulanqab 012000, Inner Mongolia, China; Corresponding author: 1572701391@qq.com

INTRODUCTION

Cancer is a disease that is highly prevalent and is defined by the uncontrolled proliferation of cells, which results in the formation of malignant tumors that can invade adjacent tissues and metastasize to distant organs through the lymphatic system or circulation. Cancer is the second most common cause of death in the world, with about 8 million cancer-related deaths and 14 million new cases each year (Ferlay *et al*. 2015). Oral cancer is a substantial public health concern, with an estimation of 275,000 new cases diagnosed worldwide each year, among a variety of malignancies. It is currently the sixth most prevalent malignancy worldwide (Warnakulasuriya 2009).

Despite ongoing progress in research and treatment strategies, oral cancer continues to be a substantial global health issue. The biomedical field is continually confronted with challenges because of the persistently low survival rates, which are primarily related to its high incidence. Tobacco consumption and excessive alcohol consumption are significant risk factors for oral cancer (Gopal *et al* 2025). Viral and fungal infections, poor oral

hygiene, immunosuppression, and protracted exposure to carcinogenic agents such as radiation, heavy metals, industrial chemicals, and inorganic acids are additional contributors (Kumar *et al*. 2016; Hernandez *et al*. 2017). Certain microbial species in the buccal cavity are suspected of promoting chronic inflammation, which has the potential to accelerate carcinogenesis (Tayyeb *et al*. 2024; Ravikumar *et al*. 2024). Additionally, the progression of the disease has been linked to opportunistic pathogens such as *Candida* species and human papillomavirus (HPV), even though HPV-related oral cancers occur in only a small percentage of cases (~2%). Among patients with oral cancer, the mortality rate is significant due to these etiological factors (Coletta *et al*. 2020). The five-year survival rate for oral cancer is approximately 60%; however, this figure can rise to 90% when the disease is detected at an early stage. Regrettably, late-stage diagnosis is a prevalent occurrence, affecting approximately 60% of patients. This is frequently the result of factors such as limited health literacy, socio-economic barriers, or delays in clinical recognition by healthcare professionals (Sujir *et al*. 2019).

Surgical excision of the tumor is the primary strategy for conventional treatment of oral cancer, which is followed by chemotherapy and radiation therapy. Despite their widespread use, these methods are frequently expensive and can have a substantial negative effect on the life of patients (Rivera 2015). The selection of a therapeutic approach is contingent upon a variety of factors, such as the tumor's anatomical location, size, histological grade, the patient's overall health status, their capacity to tolerate treatment-related adverse effects, and their personal treatment preferences (Khalid *et al* 2025). The aggressive and metastatic character of malignant cells complicates conventional therapeutic interventions and increases the likelihood of treatment failure or disease recurrence in most cases (Yao *et al*. 2020). Consequently, it is imperative to investigate innovative therapeutic strategies that are both more effective and less harmful to healthy tissues. The development of targeted therapies that selectively target malignant cells while preserving normal ones has become a primary focus of recent cancer research. In this perspective, nanotechnology presents promising solutions as an emerging and transformative field (Gomerdinger *et al* 2025). Nanocarriers have garnered significant attention as potential drug delivery systems for oral cancer therapy. Their capacity to enhance drug bioavailability, target tumor sites, and reduce systemic toxicity renders them highly advantageous. Additionally, the utilization of biofunctionalized nanofibers, which are designed with high porosity and are labelled with therapeutic biomolecules, has yielded promising outcomes in the treatment of oral cancers (Kandaswamy *et al*. 2024).

Gold nanoparticles (AuNPs) have become one of the most widely used materials among inorganic nanoparticles because of their singular combination of structural stability, biocompatibility, chemical inertness, and versatility. They are suitable for a variety of biomedical applications, particularly in cancer therapeutics, because of their well-characterized surface chemistry, which enables efficient functionalization with a wide range of biological and chemical ligands (Hu *et al*. 2020). AuNPs show minimal toxicity at low concentrations, which further enhances their suitability for clinical applications. The synthesis of nanoparticles can be succeeded through various methods. However, these conventional methods frequently involve the use of hazardous reagents and high costs, which pose significant health and environmental risks due to the toxic byproducts produced during the synthesis or stabilization processes (Santhosh *et al*. 2022). To circumvent these constraints, there has been a significant increase in green synthetic methods, particularly those that employ plant extracts. The eco-friendly and large-scale production of AuNPs can be facilitated by phytochemicals that are present in plants, which function as natural

reducing and stabilizing agents. This method reduces production costs, eliminates the need for dangerous chemicals, and minimizes the environmental impact. As a result, plant-mediated synthesis provides a more environmentally friendly, sustainable, and secure alternative to conventional nanoparticle fabrication methods (Sun *et al*. 2019).

Plants have been utilized in traditional healing practices since ancient times, and they have been an abundant reservoir of medicinal compounds. A wide range of bioactive constituents within medicinal botanicals have been identified through phytochemical investigations, with numerous examples demonstrating therapeutic potential for a wide range of health conditions (Kalita *et al*. 2012). *Lantana camara (L. camara)* is a flowering ornamental shrub that is a member of the genus *Lantana* and the species *Lantana camara* Linn. It is classified in the Magnoliopsida class of the Magnoliophyta division of the kingdom Plantae. Locally, it is referred to as "Unni chedi" in Tamil (Ghisalberti 2000; Sharma *et al*. 2007). A variety of maladies have been treated with *L. camara* in traditional folk medicine. Lantadene A and Lantadene B are significant bioactive compounds among its phytochemical constituents. Scientific investigations have verified that leaf extracts of *L. camara* demonstrate a variety of pharmacological properties, such as antioxidant, antifungal, antibacterial, anticancer, wound healing, and antidiabetic properties (Barreto *et al*. 2010; Kato-Noguchi and Kurniadie 2021). *L. camara* is presently being investigated for its potential role in oral cancer therapy due to its proven bioactivity and traditional use in treating mouth ulcers.

The present study introduces a unique plant-mediated approach for synthesizing AuNPs using *L. camara* extract, which differs from previously reported green synthesis methods in several key aspects (Al-Mafarjy *et al* 2024; Ruth *et al.* 2025). Unlike earlier studies that primarily focused on qualitative characterization, this work provides a comprehensive physicochemical and biological evaluation of the synthesized AuNPs, including UV–Vis, FTIR, XRD, TEM, SEM–EDX, and DLS analyses. Furthermore, the study demonstrates dual biological functionality both antibacterial and anticancer activities validated through ROS generation, caspase activation, and MTT assays, which have not been simultaneously reported for this plant system. The integration of quantitative statistical analysis and exact p-values enhances the scientific rigor and reproducibility compared with prior reports.

In contrast to recent publications on plant-mediated AuNP synthesis (e.g., *Azadirachta indica*, *Ocimum sanctum*, *Curcuma longa*), this work uniquely establishes a mechanistic link between nanoparticle concentration, oxidative stress induction, and apoptosis, providing new insights into the biomedical potential of phytochemical-derived AuNPs.

MATERIALS AND METHODS

Preparation of *L. camara* Extract

Fresh leaves of *L. camara* were collected from wild population in May 2025 from university garden of the south China Agricultural University campus, Guangzho. The leaves were thoroughly rinsed and air-dried in the shade. Subsequently, a clean mortar and pestle were employed to grind the desiccated leaves into powder. About 10 g of powdered leaf material and 100 mL of double distilled water were used for the extraction procedure (Kato-Noguchi and Kurniadie 2021). The release of phytochemicals was facilitated by

heating the resulting mixture at 60 °C for 15 min. The extract was filtered using Whatman No. 1 paper and stored at room temperature until use.

Green Synthesis of AuNPs

About 5 mL of the *L. camara* extract was combined with 45 mL of a 1.0 mM aqueous solution of Gold (III) chloride hydrate ($AuCl_3 \cdot H_2O$) to synthesize AuNPs. The biosynthesis was carried out at pH 7.0, under constant stirring at room temperature for 60 min. The formation of AuNPs was indicative of the reduction of Au^{3+} ions to elemental gold (Au^0) in the reaction mixture, as evidenced by a visible color change. The AuNPs were isolated by centrifuging the resulting colloidal suspension at 15,000 rpm for 30 min at 37 °C. The supernatant was discarded with care, and the settled nanoparticles were washed by re-suspending the granules in distilled water and centrifuging them again under the same conditions. The purpose of this washing phase was to eliminate any biomolecules or phytoconstituents that could potentially impede the characterization or application of the AuNPs. The purified AuNPs were stored at 4 °C in dark airtight containers to prevent aggregation and photodegradation.

Characterization

The morphological characteristics of the AuNPs were characterized using a TECNAI G2 20 TEM that was operated at 200 kV of accelerating voltage. To evaluate the shape and size distribution of particles, HR-TEM images were acquired. The identification of characteristic diffraction peaks corresponding to metallic gold was facilitated using XRD with Cu-Kα radiation. UV–visible spectroscopy was employed to investigate the optical properties of the AuNPs, which confirmed the SPR characteristic of AuNPs. The spectrophotometer utilized was a Shimadzu 1601 with a 2-mm path length quartz cuvette. The functional groups were identified *via* FTIR spectroscopy. To evaluate the colloidal stability and dispersion characteristics of the AuNPs, DLS and zeta potential analysis were carried out on a Malvern Zetasizer Nano-ZS90 instrument. The particle size distribution and surface charge were also evaluated.

Anti-cancer Activity

Cell culture

Human KB cells were cultured in Dulbecco's Modified Eagle Medium (DMEM) supplemented with 10% fetal bovine serum (FBS) and 1% antimycotic solution, as obtained from the ATCC, USA. The cells were maintained in incubator (37 °C, 5% CO_2) until they were used in in vitro anticancer evaluations.

Cytotoxicity Assay

The MTT assay was employed to assess the cytotoxic effect of the AuNPs on KB cells. To facilitate appropriate cell adherence in the growth medium, KB cells were seeded in a 96-well microplate and allowed to incubation. The cells were incubated for 24 h after adhesion and treated with various doses of AuNPs (15 to 60 µg/mL). Immediately following the treatment period, 100 µL of fresh DMEM and 20 µL of MTT solution were introduced to each well, and a 4-h incubation period was conducted to facilitate the formation of formazan crystals. Afterward, add 100 µL of DMSO to each well to dissolve the formazan crystals. The absorbance at 570 nm was measured using a microplate reader.

Measurement of ROS

The intracellular ROS generation in KB cells treated with AuNPs was assessed using DCFH-DA (2',7'-dichlorodihydrofluorescein diacetate) staining. To facilitate adherence, KB cells were dispersed in a 24-well plate in DMEM and incubated (37 °C, 24 h). Subsequently treated the cells with 25 µg/mL and 30 µg/mL of AuNPs after incubation, and they were then incubated for an additional 24 h at 37 °C. Following treatment, 10 µL of DCFH-DA staining solution was added to each well, and incubated (37 °C, 1 h) in the dark. The fluorescence microscope was used to observe the accumulation of intracellular ROS. The increased fluorescence intensity in the AuNPs treated groups compared to the untreated controls indicated elevated ROS levels.

Acridine Orange/Ethidium Bromide (AO/EB) Staining

The AO/EB dual staining was implemented to evaluate apoptotic cell death in KB cells that were treated with AuNPs. To facilitate adherence, KB cells were dispersed in a 24-well plate in DMEM and incubated (37 °C, 24 h). Following this, the cells were incubated for an additional 24 h under the same conditions and treated with 25 µg/mL and 30 µg/mL of AuNPs. The cells were stained with a 1:1 ratio of AO/EB for 5 min at 37 °C immediately following treatment. The nuclear morphology and membrane integrity of the stained cells were subsequently analyzed using a fluorescence microscope to distinguish between viable, apoptotic, and necrotic populations.

Propidium Iodide Staining

The apoptotic morphological alterations in KB cells treated with AuNPs were visualized using propidium iodide (PI)-staining. KB cells were inoculated in 24-well plates in DMEM and incubated (37 °C, 24 h). The cells were subsequently incubated for an additional 24 h under the same conditions and treated with 25 µg/mL and 30 µg/mL of AuNPs. After treatment, 5 µL of PI staining solution was added and incubated in the dark for 20 min at room temperature. Examined the stained cells using a fluorescence microscope to evaluate their apoptotic characteristics. In the AuNPs-treated groups, PI staining demonstrated chromatin condensation and nuclear fragmentation, which suggests apoptotic cell death.

Caspases Activity

Commercial enzyme activity assay kits were employed to quantify the activity levels of caspase-3, caspase-8, and caspase-9 in control and AuNPs treated KB cells, in accordance with the manufacturer's guidance. The KB cells were treated with AuNPs at designated concentrations. KB oral cancer cells were inoculated in 6-well plates for flow cytometric analysis of caspase-3, caspase-8, and caspase-9 expression. The cells were washed with PBS, and the culture medium was disposed at the conclusion of the treatment period.

The cells were subsequently fixed by incubating them momentarily at 4 °C and adding 1.0 mL of pre-chilled 70% ethanol. The cells were centrifuged at high speed after fixation, and the supernatant was meticulously aspirated to prevent the particle from being disturbed. The particles were washed twice with PBS, and 5 µL of FITC-conjugated caspase antibody was subsequently added. The samples were thoroughly mixed and incubated in the dark (20–25 °C, 30 min). Following incubation, the cells were rinsed once with 1× PBS containing 0.1% sodium azide to eliminate any remaining unbound antibody.

Lastly, the cells were resuspended in 0.5 mL of PBS, thoroughly mixed, and analyzed using flow cytometry to quantify caspase-3-positive cells, which demonstrates apoptosis.

Anti-bacterial Activity

The antibacterial capabilities of the AuNPs were evaluated in relation to two bacterial strains *Escherichia coli* (*E. coli*) and *Staphylococcus aureus (S. aureus)*. The nutrient agar was prepared by dissolving the appropriate quantity in distilled water and subsequently sterilizing it through autoclaving. The medium was subsequently poured into Petri plates and permitted to solidify.

Sterile swabs were employed to uniformly distribute bacterial cultures across the solidified nutrient agar surface. Sterile 6 mm filter paper discs were supplied with 5 µL of the AuNPs solution for the assay. These discs were subsequently affixed to the inoculated agar plates. The dishes were incubated (37 °C, 24 h). The efficacy of AuNPs against the respective bacterial strains was determined by measuring the diameter of the zone of inhibition (ZOI) formed around each disc, which was used to determine antibacterial activity.

Statistical Analysis

All experiments were performed in triplicate ($n = 3$) using independent biological replicates. Data was analyzed using GraphPad Prism v10.0 (GraphPad Software) and Excel used to perform all the statistical analyses. Analysis was done in triplicate, and we use mean for statistical analysis. One-way ANOVA test helps in determination of Statistical significance, succeeded by post hoc Tukey test. $P < 0.05$. was the fixed statistical significance.

RESULTS AND DISCUSSION

UV–Visible Spectroscopy

Surface plasmon resonance (SPR) is a distinctive optical property of AuNPs, producing a characteristic absorption band in the visible region, typically between 500 nm and 600 nm, that can be effectively monitored using UV–visible spectroscopy. In this study, the *L. camara* extract alone exhibited a broad absorbance in the UV region and a minor shoulder in the visible range, attributable to its phytochemical constituents. Upon addition of $HAuCl_4$, however, a new, sharp SPR peak appeared at 568 nm, confirming the formation of AuNPs.

A gradual red shift in the SPR peak was observed during synthesis, consistent with binding of plant biomolecules to the nanoparticle surface and the resulting increase in local refractive index (Ruth *et al* 2025). The SPR absorbance intensity stabilized after approximately 10 min, indicating that nucleation and growth of AuNPs had reached a steady state under the experimental conditions.

While this stabilization reflects completion of particle formation dynamics, it does not alone confirm full reduction of Au^{3+} ions. The inference of near-completion was supported by the concurrent colour change and the absence of further spectral evolution beyond 10 min, together suggesting that most Au^{3+} ions were reduced to Au^0 (Al-Mafarjy *et al* 2024).

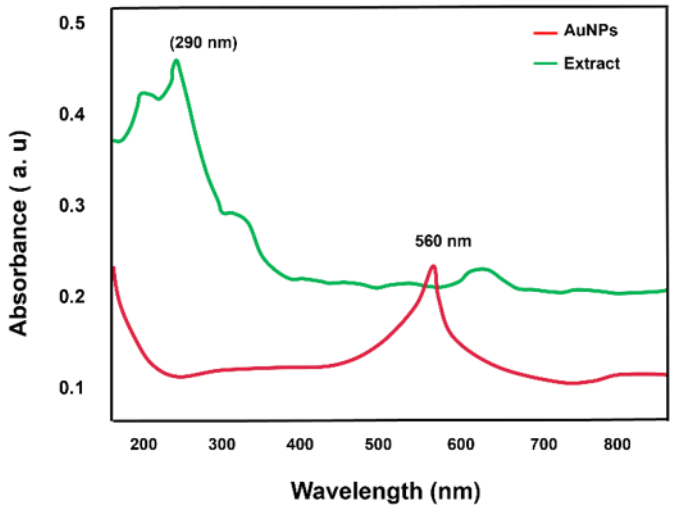

Fig. 1. UV-Visible spectra of *L. camara* extract and *L. camara* mediated AuNPs

Fourier Transform Infra-Red Spectroscopy

The FTIR spectra of the *L. camara* extract and the AuNPs are depicted in Fig. 2 and Table 1. The FTIR profile of the *L. camara* extract demonstrated the presence of a variety of functional groups that are involved in the reduction and stabilization of gold ions, as evidenced by the presence of several characteristic absorbance bands (Pasieczna-Patkowska *et al* 2025; Patil *et al* 2024). The peaks at 950 and 1190 cm^{-1} were the most prominent, indicating –C–F stretching vibrations. The peaks at 1354 cm^{-1} were attributed to –C–O–C stretching of ether linkages. The peaks at 1497 cm^{-1} were indicative of aromatic –C=C stretching. The peaks at 3001 cm^{-1} were representative of –C–H stretching vibrations. In contrast, the FTIR spectrum of the AuNPs exhibited substantial absorbance bands at 1498 cm^{-1} (aromatic –C=C) and a slightly displaced peak at 3010 cm^{-1}, which was associated with =C–H stretching. This suggests that these functional groups are involved in the bio-reduction and capping of AuNPs, as evidenced by their presence in both spectra. The interaction between gold ions and phytochemicals from *L. camara* during nanoparticle formation is also supported by the disappearance or displacement of specific peaks.

Table 1. FTIR Peak Assignments of *L. camara* Extract and AuNPs

Wavenumber (cm^{-1})	Functional group	Assignment	Sample name
950	–C–F stretching	Fluoro group vibrations	*L. camara* extract
1190	–C–F stretching	Fluoro group vibrations	*L. camara* extract
1354	–C–O–C stretching	Ether linkage	*L. camara* extract
1497	Aromatic –C=C stretching	Aromatic ring vibrations	*L. camara* extract
3001	–C–H stretching	Alkyl C–H bonds	*L. camara* extract
1498	Aromatic –C=C stretching	Aromatic ring vibrations	AuNPs
3010	=C–H stretching	Alkenyl C–H bonds	AuNPs

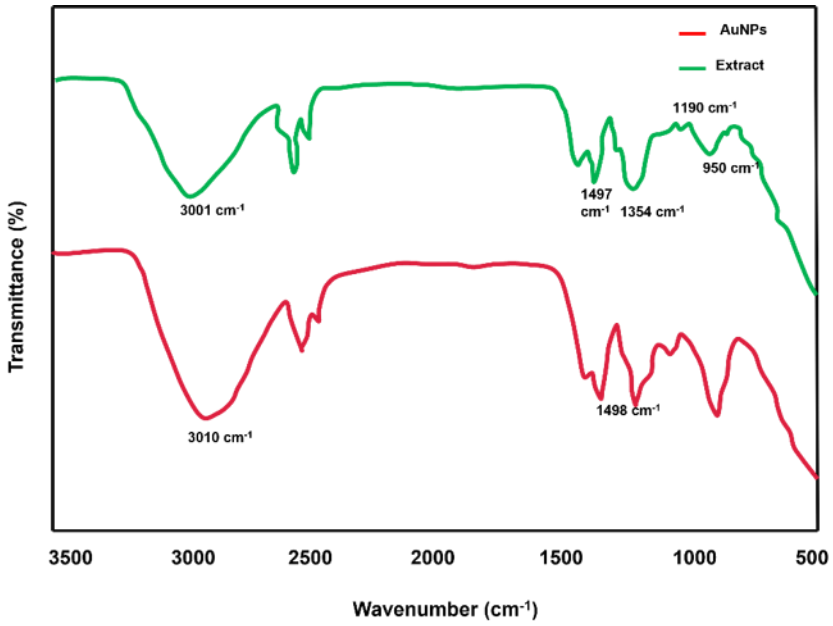

Fig. 2. FTIR spectra of *L. camara* extract and *L. camara* mediated AuNPs

Transmission Electron Spectroscopy

The size, morphology, and structural characteristics of the AuNPs were analyzed using HR-TEM. The nanoparticles primarily demonstrated a spherical morphology. The average particle diameter was between 40 and 80 nm, as illustrated in Fig. 3. The particle size distribution, obtained by measuring over 100 particles using ImageJ software, indicated an average diameter of 65.4 ± 12.7 nm, consistent with the TEM micrographs (Fig. 3). The particle size histogram confirmed a narrow distribution, suggesting homogeneous nucleation during biosynthesis. The HRTEM images demonstrated lattice fringes that were well-resolved, with an interplanar spacing of approximately 0.21 nm. This fringe spacing is in close agreement with the (111) crystal planes of face-centered cubic (FCC) gold crystals, which typically exhibit a spacing of 0.235 nm, as per previous reports (D'Souza *et al*. 2018). These results substantiate the biosynthesized AuNPs' high structural integrity and crystalline nature.

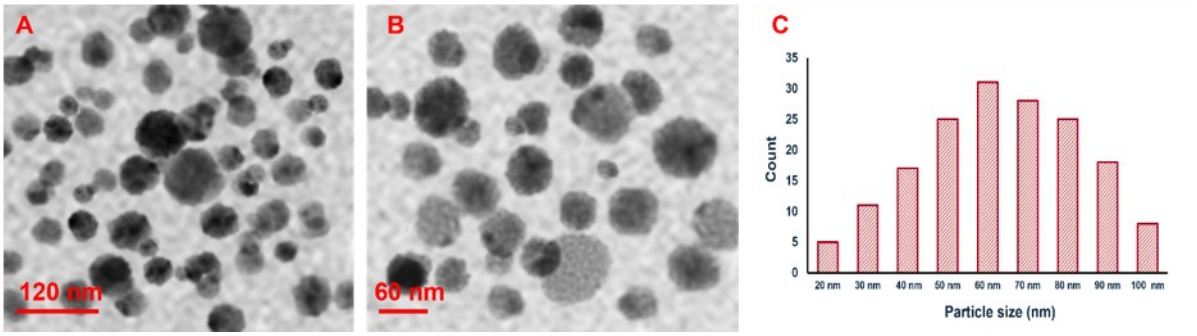

Fig. 3. TEM images AuNPs synthesized using *L. camara*

Scanning Electron Microscopy (SEM) and Selected Area Electron Diffraction (SAED)

AuNPs demonstrated homogenous spherical morphology with well-defined and regular surface features, as confirmed by SEM analysis (Fig. 4A). The images

demonstrated a uniform distribution of particles, suggesting that the sample was consistent in terms of size and shape. The crystallinity of the AuNPs was further corroborated by a structural analysis using SAED. This was demonstrated by the distinct diffraction rings that corresponded to the characteristic planes of FCC gold (Fig. 4B).

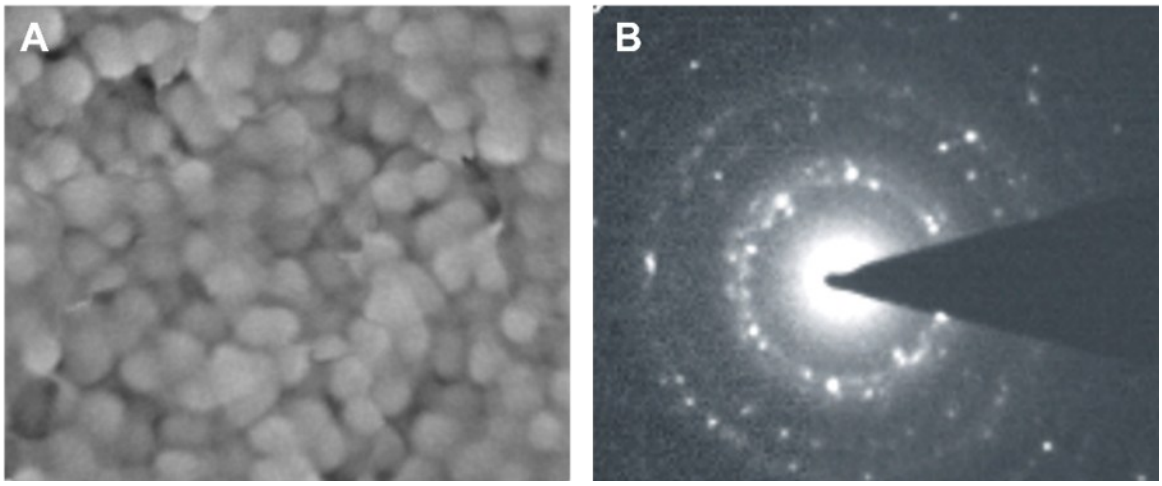

Fig. 4. SEM image (A); and SAED pattern (B) of AuNPs synthesized using *L. camara*

X-Ray Diffraction

AuNPs are illustrated in Fig. 5 by their XRD pattern. The diffractogram exhibits five prominent peaks at 38.3°, 44.5°, 64.8°, 77.7°, and 81.6°. These peaks correspond to the (111), (200), (220), (311), and (222) crystallographic planes, respectively. As per JCPDS file no. 04-0784, these diffraction peaks are in accordance with the FCC structure of metallic gold.

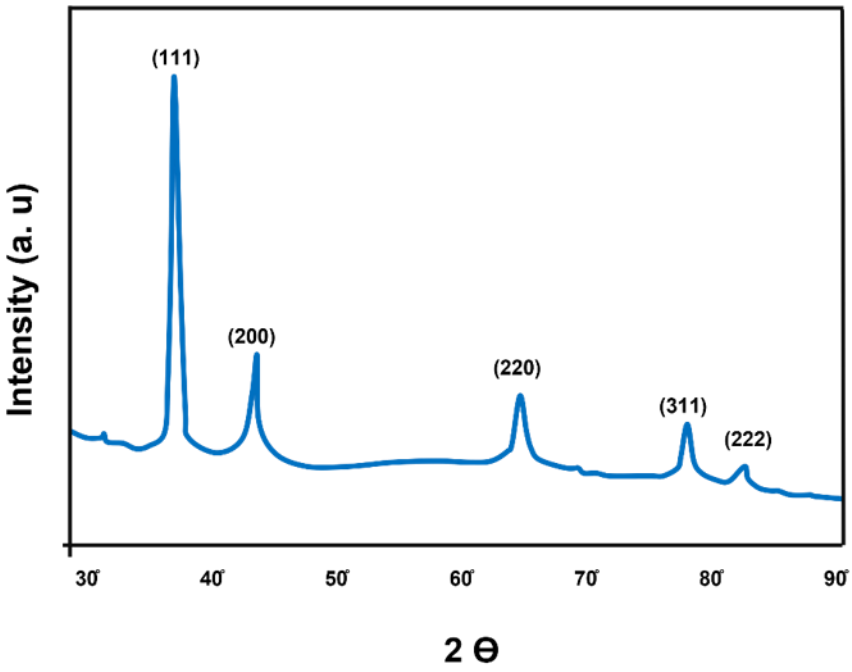

Fig. 5. XRD pattern of AuNPs synthesized using *L. camara*

The peak at 38.3°, which corresponds to the (111) plane, is the most intense among these reflections, indicating a preferential crystalline orientation in the (111) direction. The high crystallinity and phase integrity of the synthesized nanoparticles are indicated by the dominant (111) facet, which is typical for AuNPs. The average crystallite size calculated using the Scherrer equation. $D = K\lambda / (\beta \cos\theta)$ was 21-25 nm, confirming the crystalline nature of the biosynthesized AuNPs. The lattice fringe spacing observed in HR-TEM (≈ 0.21 nm) closely matched the (111) plane of FCC gold (0.235 nm), corroborating high structural integrity and crystallinity.

Energy-Dispersive X-ray Spectroscopy

The elemental composition of the biosynthesized AuNPs was analyzed using EDX spectroscopy (Fig. 6). The spectrum exhibited intense signals corresponding to elemental gold, confirming successful nanoparticle formation. A carbon peak was also detected, indicating the presence of organic molecules from *L. camara* extract adsorbed on the nanoparticle surface, which likely acted as reducing and capping agents. The apparent copper peaks observed in the spectrum originate from the copper grid used as the substrate during TEM/EDX analysis, rather than from the sample itself. This is a well-known artifact in EDX characterization, as the Cu grid contributes background signals that can overlap with Au peaks due to their close energy positions. The dominant Au signals and absence of other metallic impurities confirm the purity and successful synthesis of the AuNPs.

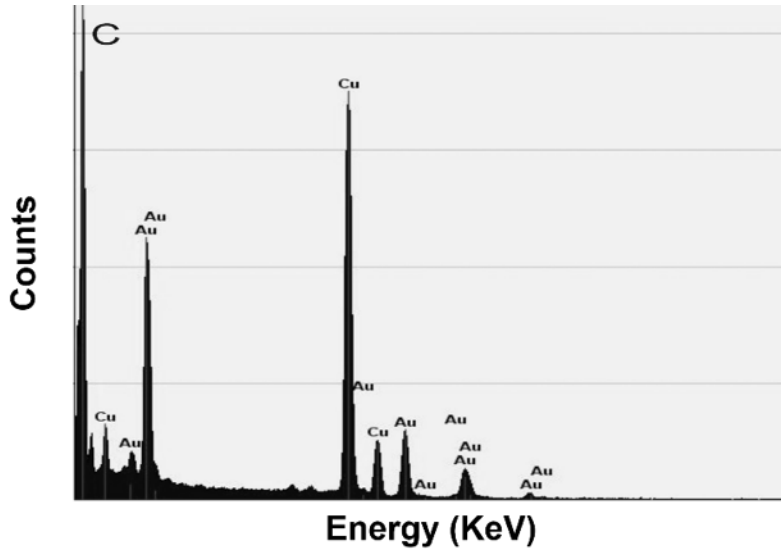

Fig. 6. EDX analysis of AuNPs synthesized using *L. camara*

Zeta and Dynamic Light Scattering

The synthesized AuNPs exhibited a zeta potential of −24.3 mV (Fig. 7A), which helps explain their moderate colloidal stability. The negative surface charge promotes electrostatic repulsion among nanoparticles, thereby reducing aggregation and enhancing dispersion stability (Gunupuru *et al* 2025). In addition to electrostatic effects, partial stabilization may also arise from steric hindrance provided by biomolecules and biosurfactants derived from *L. camara* extract, which act as capping agents on the nanoparticle surface. Interestingly, nanoparticles with slightly lower negative surface charge often show improved cellular uptake, as reduced electrostatic repulsion facilitates membrane interaction and internalization (Raj *et al*. 2018). The average hydrodynamic

diameter of the AuNPs 71.2 ± 15.2 nm and a polydispersity index (PDI) of 0.214, as determined by DLS analysis (Fig. 7B), confirming a monodisperse distribution and successful bio-reduction synthesis (Rahman *et al*. 2022).

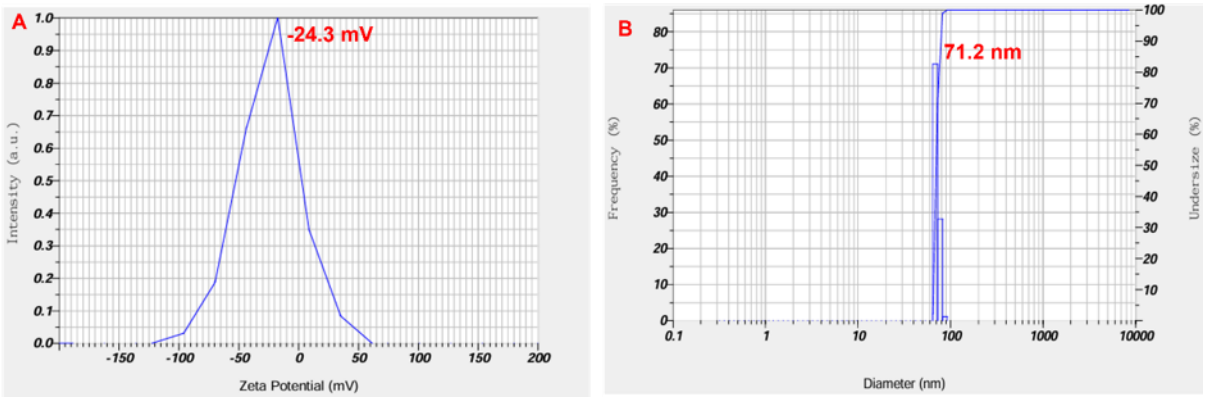

Fig. 7. Zeta potential (A); and DLS (B) of AuNPs synthesized using *L. camara*

Cytotoxicity

The MTT assay was employed to evaluate the inhibitory potential of the AuNPs on KB cell viability. As shown in Fig. 8A, the viability of KB cells decreased significantly with increasing AuNP concentration compared to the untreated control.

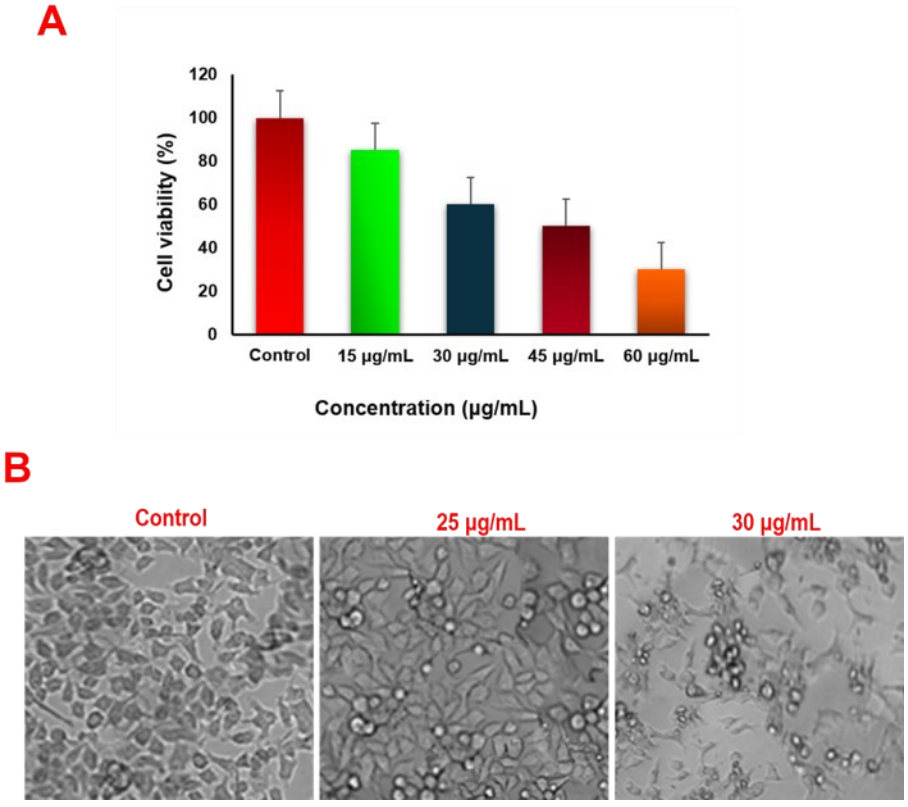

Fig. 8. (A) Cell viability of KB cells treated with AuNPs at concentrations of 15, 30, 45, and 60 µg/mL, determined by MTT assay. Data represent mean ± SD from three independent biological replicates ($p < 0.05$, $p < 0.01$, $p < 0.01$, $p < 0.01$ *vs.* control). (B) Representative microscopic images showing morphological alterations in KB cells after treatment with AuNPs at 25 and 30 µg/mL compared with untreated control.

At 25 µg/mL and 30 µg/mL, cell viability was reduced to approximately 50 %, corresponding to an IC_{50} value of 30 µg/mL. The dose-dependent decline in viability confirms the cytotoxic efficacy of the nanoparticles. Microscopic observations (Fig. 8B) further revealed morphological alterations such as cell shrinkage, membrane detachment, and apoptotic features, substantiating the inhibitory effect of AuNPs on KB cell proliferation. These results are consistent with recent reports of green-synthesized AuNPs exhibiting dose-dependent cytotoxicity (Martínez-Saráoz *et al.* 2025).

ROS Activity

ROS levels in AuNPs treated KB cells are elaborated on Fig. 9. The untreated control cells exhibited minimal green fluorescence, suggesting a low basal level of ROS. In contrast, KB cells that were exposed to AuNPs at 25 µg/mL and 30 µg/mL exhibited a profound increase in intracellular ROS levels, as evidenced by the intense green fluorescence. These findings verify that the oxidative stress within KB cells was significantly elevated following treatment with the synthesized AuNPs. The intrinsic apoptotic pathway is activated by the release of cytochrome-c from mitochondria into the cytosol, which is a known mechanism by which elevated ROS levels initiate apoptosis (Chang *et al*. 2021). The present results are consistent with this mechanism, as they demonstrate that AuNPs induce ROS-mediated cytotoxicity in KB cells, thereby contributing to their anticancer potential.

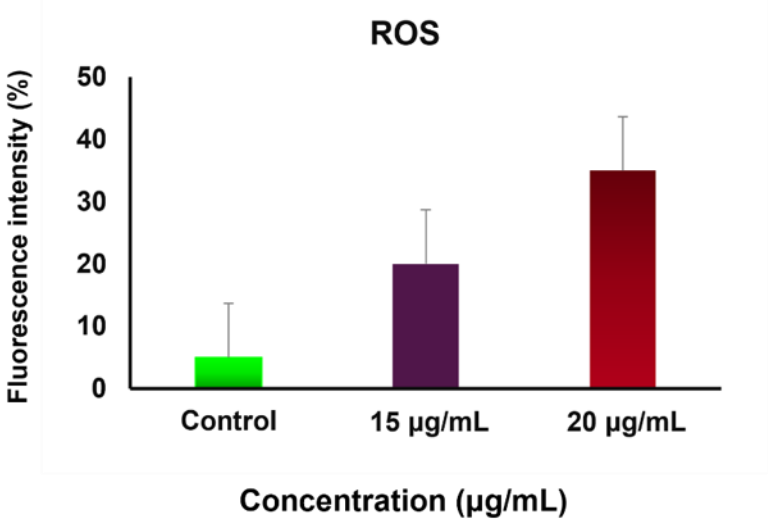

Fig. 9. Effect of AuNPs on ROS generation in the oral cancer KB cells. With significance of ($p < 0.01$, $p < 0.001$ *vs.* control). The increase in ROS levels indicates oxidative stress induced by AuNP exposure.

Live/Dead Staining

The results of the pro-apoptotic effect of AuNPs on KB cells were further validated using AO/EB dual staining, as illustrated in Fig. 10. Viable cells with intact membranes and no signs of apoptosis were shown by the strong green fluorescence of KB cells in the control group. On the other hand, the cells that were treated with 25 and 30 µg/mL of AuNPs exhibited an increase in yellow to orange fluorescence, which is indicative of early and late apoptotic cells, individually. These results corroborate that apoptosis is induced by AuNPs in a dose-dependent manner. Liu *et al*. (2015) reported that the AO/EB staining technique is effective in distinguishing between viable and apoptotic cells, thereby corroborating its utility in evaluating nanoparticle-induced cytotoxicity.

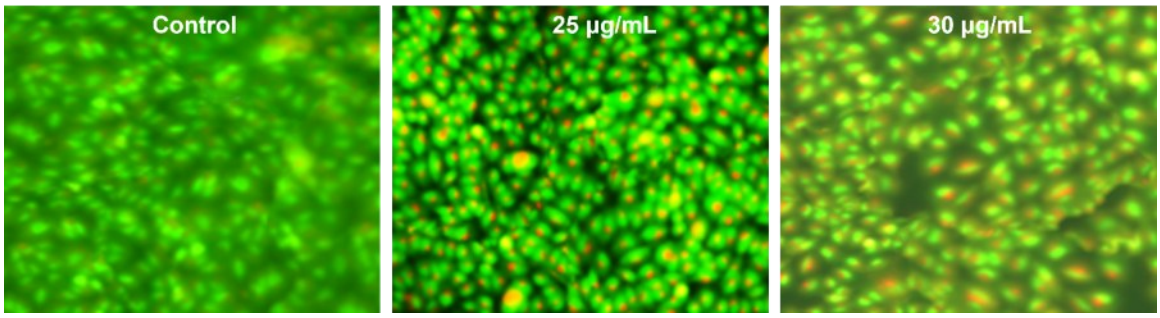

Fig. 10. Effect of AuNPs on apoptotic cell death in the oral cancer KB cells

Apoptotic Changes

The apoptotic staining of KB cells treated with AuNPs is depicted in Fig. 11, as observed through PI staining. The control cells exhibited modest red fluorescence, which suggested the absence of apoptosis and minimal membrane compromise. In contrast, KB cells treated with 25 and 30 µg/mL of AuNPs exhibited intensified red fluorescence, a symptom of apoptotic cell death that is the result of increased membrane permeability and nuclear damage.

The function of AuNPs in promoting apoptotic pathways is further validated by the enhanced red fluorescence in treated groups, which supports their anticancer potential.

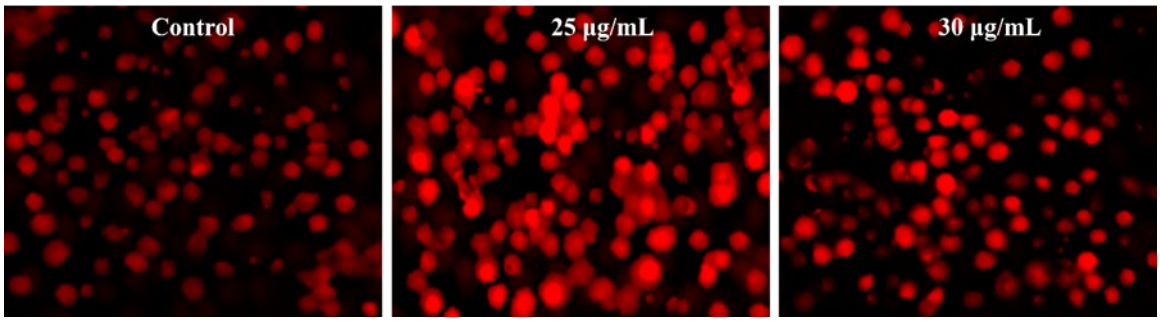

Fig. 11. PI staining showing intensified red fluorescence in AuNP-treated KB cells, indicating apoptosis compared to control

Caspases Activity

The results of the enzymatic activities of caspase-3, caspase-8, and caspase-9 in control and AuNPs treated KB cells are illustrated in Fig. 12. The control group demonstrated baseline caspase activity, which suggests that apoptotic signaling was minimal, as demonstrated.

Conversely, KB cells that were given AuNPs at doses of 25 and 30 µg/mL exhibited significantly increased levels of caspase activities. These results indicate that AuNPs effectively activated both intrinsic (caspase-9) and extrinsic (caspase-8) apoptotic pathways, which ultimately resulted in the activation of executioner caspase-3. The apoptosis-inducing potential of the AuNPs in KB cells was confirmed by the upregulation of caspase activity.

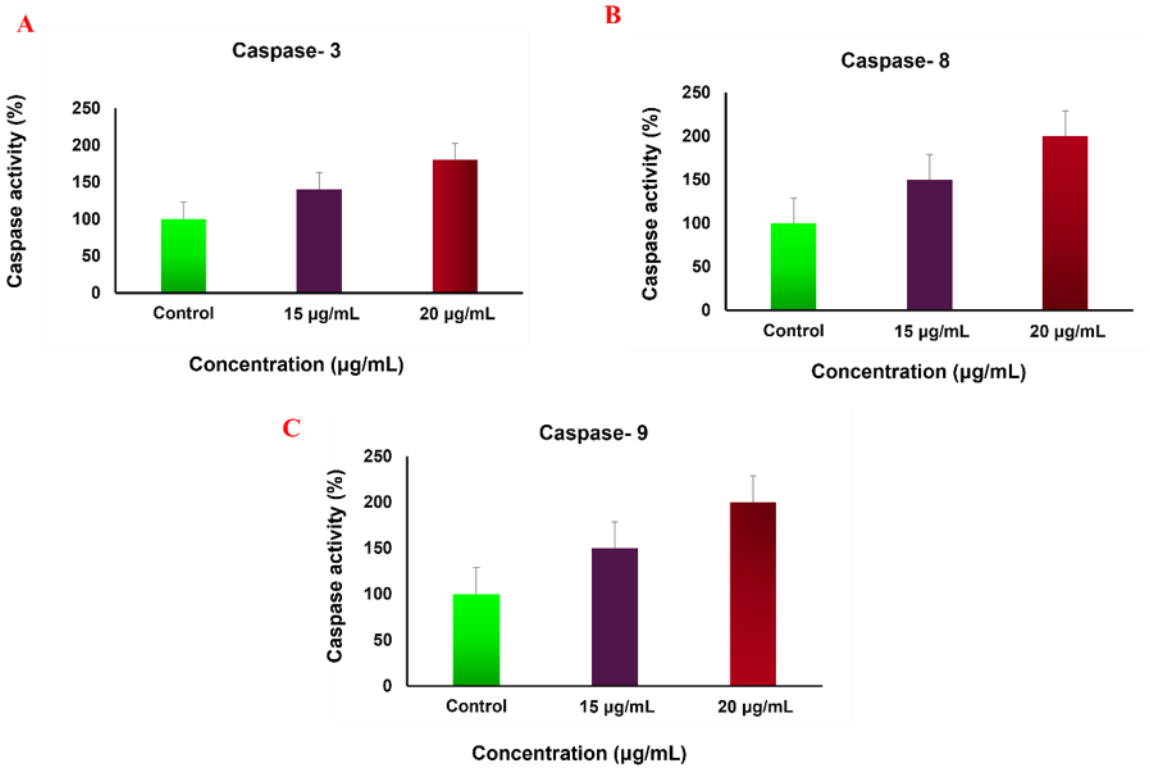

Fig. 12. Caspase activation in KB cells is treated with AuNPs. (A) Caspase-3, (B) Caspase-8, and (C) Caspase-9 activities increased significantly in a dose-dependent manner. Bars represent mean ± SD (n = 3). ($p < 0.01$, $p < 0.01$, $p < 0.001$ vs control).

Anti-microbial Activity

The antimicrobial activity of the AuNPs was assessed against both Gram-positive and Gram-negative bacterial genotypes. The results are visually depicted in Fig. 13, and the Zones of Inhibition (ZOIs) are summarized in Table 1. AuNPs labelled as 5 exhibited the most potent antibacterial activity among the tested samples, demonstrating the largest inhibition zones. The assay conditions were validated by the production of a 23-mm inhibition zone. *S. aureus* exhibited significantly larger inhibition zone than the *E. coli*. This implies that AuNPs have more potent antibacterial properties against Gram-positive bacteria. The increased efficacy may be attributed to the relatively more permeable cell walls of Gram-positive bacteria and the stronger surface interactions between the negatively charged AuNPs (zeta potential = −21 mV). In contrast, the interaction between nanoparticles and the outer membrane of Gram-negative bacteria is likely to be reduced by electrostatic repulsion.

The discharge of ionic gold (Au^{+}) from the nanoparticle surface is the mechanism of antibacterial action. This substance can penetrate bacterial cell walls, disrupt ATP synthesis, and inhibit DNA replication. Upon entering the cytoplasm, Au^{+} ions interact with thiol (−SH) groups of cellular proteins, resulting in metabolic dysfunction through disrupted proton gradients and impaired respiratory activity, and compromising membrane integrity (Anbu *et al*. 2020).

The AuNPs synthesized in this study exhibited superior antibacterial activity, against *S. aureus* and *E. coli*, in comparison to previously reported green-synthesized AuNPs, including those produced using *Lignosus rhinocerotis*, *Uncaria gambir*, and macadamia nut shells, which exhibited inhibition zones in the range of 8 to 10 mm at higher

concentrations (Arifianto *et al*. 2025; Katas *et al*. 2019; Arief *et al*. 2020). The increased antimicrobial activity observed in this study is likely influenced by factors such as the nature of the capping agents used during green synthesis, particle size, degree of surface functionalization, and surface chemistry (Barabadi *et al*. 2020; Saravanan *et al*. 2021). Furthermore, the shorter synthesis time offers practical advantages in terms of applicability and scalability. Future studies will include MIC and MBC determinations using broth microdilution, providing quantitative measures of bacteriostatic and bactericidal activity and enabling stronger comparisons with recent reports.

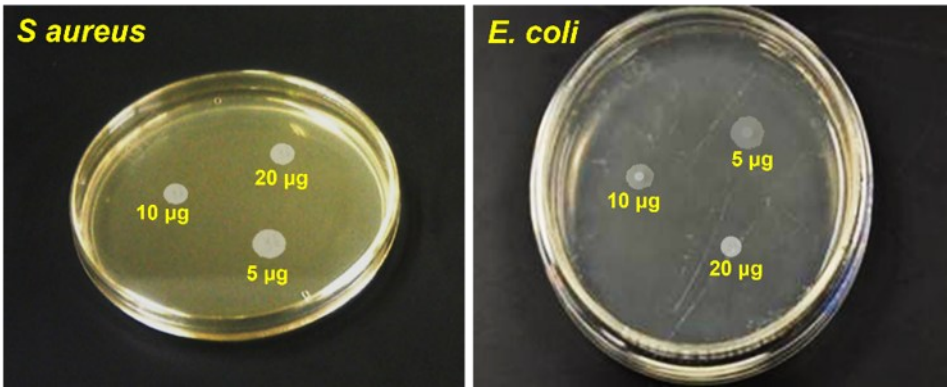

Fig. 13. Anti-bacterial activity of AuNPs against *S. aureus* and *E. coli*

Table 1. Anti-bacterial Activities (zones of Inhibition) of AuNPs at Concentrations of 5, 10, and 20 µg

Tested Bacteria	Inhibition Zone by Tested Sample (mm)		
	AuNPs (5 µg)	AuNPs (10 µg)	AuNPs (20 µg)
S. aureus	18 ± 0.5	20 ± 0.3	23 ± 0.2
E. coli	10 ± 0.4	12 ± 0.3	15 ± 0.2

These results emphasize the potential of *L. camara* mediated AuNPs as a prospective novel anticancer agent for the treatment of oral cancer. To completely elucidate the detailed molecular mechanisms that underlie the anticancer effects of these AuNPs and to validate their therapeutic potential in clinical applications, additional in-depth studies are required.

CONCLUSION

This study successfully demonstrated the green synthesis of gold nanoparticles (AuNPs) using *L. camara* extract, establishing a sustainable and eco-friendly route for nanoparticle fabrication. This was confirmed by UV–Vis, FTIR, TEM, SEM, SAED, XRD, EDX, zeta potential, and DLS analyses.

1. The nanoparticles exhibited spherical morphology. The average particle diameter was between 40 and 80 nm. The nanoparticles exhibited strong crystallinity with FCC (111) orientation.

2. AuNPs showed moderate colloidal stability and monodispersity, supported by phytochemical capping agents.
3. They demonstrated dose-dependent cytotoxicity in KB oral cancer cells, inducing reactive organic species (ROS) generation and caspase-mediated apoptosis.
4. Significant antibacterial activity was observed, particularly against *S. aureus*, highlighting dual biomedical potential.
5. Future studies will expand cytotoxicity testing to normal and additional cancer cell lines, employ advanced molecular assays (Annexin V/PI, mitochondrial potential, Western blot), determine MIC/MBC for antibacterial activity, and validate efficacy and biocompatibility *in vivo* with scalable synthesis optimization.

ACKNOWLEDGEMENTS

Conflict of Interest

Authors have declared that no conflict of interest is associated with this work.

Funding

There is no Funding available for this work

Data availability

The data associated with the findings of this study are available from the corresponding authors, upon reasonable request.

REFERENCES CITED

Al-Mafarjy, S. S., Nursakinah, S., Naser M. A., Daruliza, K., Alkatib, H. H., and Dheyab, A. M. (2024). "Green synthesis of gold nanoparticles using *Coleus scutellarioides* leaf extract and their characterization," *Inorganic Chemistry Communications* 161, article 112052. https://doi.org/10.1016/j.inoche.2024.112052

Anbu, P., Gopinath, S.C.B., and Jayanthi, S. (2020). "Synthesis of gold nanoparticles using Platycodon grandiflorum extract and its antipathogenic activity under optimal conditions," *Nanomater Nanotechnol* 10, 1-9. https://doi.org/10.1177/1847980420961697

Arief, S., Nasution, F.W., and Labanni, A. (2020). "High antibacterial properties of green synthesized gold nanoparticles using *Uncaria gambir* Roxb leaf extract and triethanolamine," *J. Appl. Pharm. Sci.* 10, 124-130. https://doi.org/10.7324/JAPS.2020.10814

Arifianto, D., Astuti, S., Lusiani, B. Zaidan, A.H., Winarno, W., Yaqubi, A.K., Susilo, Y., Qadir, K.W., and Syahrom, A. (2025). "Photodynamic antibacterial activity of green-synthesized gold nanoparticles from mangosteen peel extract using blue laser irradiation," *Lasers Med. Sci.* 40, article 305. https://doi.org/10.1007/s10103-025-04549-x

Barabadi, H., Vahidi, H., Damavandi K. K., Rashedi, M., and Saravanan, M. (2020). "Antineoplastic biogenic silver nanomaterials to combat cervical cancer: A novel

approach in cancer therapeutics," *J. Clust. Sci.* 31, 659-672. https://doi.org/10.1007/s10876-019-01697-3

Barreto, F. S., Sousa, E. O., Campos, A. R., Costa, J. G. M., and Rodrigues, F. F. G. (2010). "Antibacterial activity of *Lantana camara* Linn and *Lantana montevidensis* Brig extracts from Cariri-Ceará, Brazil," *Journal of Young Pharmacists* 2, 42-44. https://doi.org/10.4103/0975-1483.62211

Chang, Y., Zheng, C., Chinnathambi, A., Alahmadi, T. A., and Alharbi, S. A. (2021). "Cytotoxicity, anti-acute leukemia, and antioxidant properties of gold nanoparticles green-synthesized using *Cannabis sativa* L. leaf aqueous extract," *Arabian Journal of Chemistry* 14, article 103060. https://doi.org/10.1016/j.arabjc.2021.103060

Coletta, R. D., Yeudall, W. A., and Salo, T. (2020). "Grand challenges in oral cancers," in: *Frontiers in Oral Health* 1, 3. https://doi.org/10.3389/froh.2020.00003

D'Souza, S., and Addepalli, V. (2018). "Preventive measures in oral cancer: An overview," in: *Biomedicine and Pharmacotherapy* 107, 72-80. https://doi.org/10.1016/j.biopha.2018.07.114

Ferlay, J., Soerjomataram, I., Dikshit, R., Eser, S., Mathers, C., Rebelo, M., Parkin, D. M., Forman, D., and Bray, F (2014). "Cancer incidence and mortality worldwide: Sources, methods and major patterns in GLOBOCAN 2012," *International Journal of Cancer* 136, E359-E386. https://doi.org/10.1002/ijc.29210

Ghisalberti, E. L. (2000) "*Lantana camara L.* (Verbenaceae)," *Fitoterapia* 71, 467-486. https://doi.org/10.1016/S0367-326X(00)00202-1

Gomerdinger, V. F., Nabar, N., and Hammond, P. T. (2025). "Advancing engineering design strategies for targeted cancer nanomedicine," *Nat. Rev. Cancer* 25, 657-683. https://doi.org/10.1038/s41568-025-00847-2

Gopal, A., Palaniraja, S., K, D., Dhyani, V., Kulkarni, M., Guddattu, V. (2025). "Dose-response relationship of tobacco smoking and alcohol consumption on oral cancer: A systematic review and meta-analysis," *Annals of Oncology 36,* 0923-7534. https://doi.org/10.1016/j.annonc.2025.10.1131

Gunupuru, R., and Paul, P. (2025). "Synthesis and characterization of 2-amino-5-mercapto-1,3,4-thiadiazole functionalized gold nanoparticles and its use for colorimetric sensing of Cr^{3+} and Pb^{2+} in aqueous medium," *Journal of the Indian Chemical Society* 105, article 101566. https://doi.org/10.1016/j.jics.2025.101566

Hernandez, B. Y., Zhu, X., Goodman, M. T., Gatewood, R., Mendiola, P., Quinata, K., and Paulino, Y. C (2017). "Betel nut chewing, oral premalignant lesions, and the oral microbiome," *PLoS One* 12(2), article e0172196. https://doi.org/10.1371/journal.pone.0172196

Hu, X., Zhang, Y., Ding, T., Liu, J., and Zhao, H. (2020). "Multifunctional gold nanoparticles: A novel nanomaterial for various medical applications and biological activities," *Frontiers in Bioengineering and Biotechnology* 8, 990. https://doi.org/10.3389/fbioe.2020.00990

Kalita, G. S., Loganathan, K., and Bhaskara Rao, K. V. (2012). "A review on medicinal properties of *Lantana camara* Linn," *Res J Pharm Technol* 5, 711-715.

Kandaswamy, K., Subramanian, R., Giri, J., Subramanian, R., Giri, J., Guru, A., and Arockiaraj, J. (2024). "A robust strategy against multi-resistant pathogens in oral health: Harnessing the potency of antimicrobial peptides in nanofiber-mediated therapies," *International Journal of Peptide Research and Therapeutics* 30(3), 1-17. https://doi.org/10.1007/s10989-024-10613-x

Katas, H., Lim, C. S., Nor Azlan, A. Y. H., Buang, F., and Busra, M. F. (2019). "Antibacterial activity of biosynthesized gold nanoparticles using biomolecules from *Lignosus rhinocerotis* and chitosan," *Saudi Pharm J* 27, 283-292. https://doi.org/10.1016/j.jsps.2018.11.010

Kato-Noguchi, H., and Kurniadie, D. (2021). "Allelopathy of *Lantana camara* as an invasive plant," *Plants* 10(5), article 1028. https://doi.org/10.3390/plants10051028

Khalid, M., Rehman, M., Yi-Feng W., Xing-Jie L. (2025). "Recent advances in nanopharmaceutical strategies for cancer treatment," *Biochemical and Biophysical Research Communications* 676(1), 45-56. https://doi.org/10.1016/j.bbrc.2025.152249

Kumar, M., Nanavati, R., Modi, T. G., and Dobariya, C. (2016). "Oral cancer: Etiology and risk factors: A review," *Journal of Cancer Research and Therapy* 12(2), 458-463. https://doi.org/10.4103/0973-1482.186696

Liu, K., Liu, P.C., Liu, R., and Wu, X. (2015). "Dual AO/EB staining to detect apoptosis in osteosarcoma cells compared with flow cytometry," *Med Sci Monit Basic Res* 21, 15-20. https://doi.org/10.12659/MSMBR.893327

Martínez-Saráoz, J. V., Longoria-García, S., Gallardo-Blanco, H. L., Sánchez-Domínguez, C. N., and Sánchez-Domínguez, M. (2025). "Impact of methodological variations on MTT assay for gold nanoparticle toxicity evaluation," *Springer Proceedings in Materials* 85. https://doi.org/10.1007/978-3-031-99987-1_1

Pasieczna-Patkowska, S., Cichy, M., and Flieger, J. (2025). "Application of Fourier transform infrared (FTIR) spectroscopy in characterization of green synthesized nanoparticles," *Molecules* 30, article 684. https://doi.org/10.3390/molecules30030684

Patel, K., Patil, M., Abhale, Y., Dateer, R. B., Kumar, D., Pérez Larios, A., Chauhan, A., Jabir, M. S., and Ghotekar, S. (2024). "A critical review on *Lantana camara* extract-mediated bio-inspired synthesis of nanomaterials and their potential application: Challenges and future perspectives," *Inorganic Chemistry Communications* 161, article 113830. https://doi.org/10.1016/j.inoche.2024.113830

Rahman, T. U., Khan, H., Liaqat, W., and Zeb, M. A. (2022). "Phytochemical screening, green synthesis of gold nanoparticles, and antibacterial activity using seed extract of *Ricinus communis* L.," *Microscopy Research and Technique* 85, 202-208. https://doi.org/10.1002/jemt.23896

Raj, S., Mali, S. C., and Trivedi, R. (2018). "Green synthesis and characterization of silver nanoparticles using *Enicostemma axillare* (Lam.) leaf extract," *Biochemical and Biophysical Research Communications* 503, 2814-2819. https://doi.org/10.1016/j.bbrc.2018.08.045

Ravikumar, S., Inbaneson, S. J., Suganthi, P., and Gnanadesigan, M. (2024). "Zinc oxide nanoparticles functionalized with cinnamic acid for targeting dental pathogen receptors and modulating apoptotic genes in human oral epidermal carcinoma KB cells," *Molecular Biology Reports* 51, article 352. https://doi.org/10.1007/s11033-024-09289-9

Rivera, C. A. (2015). "The challenge of the state of susceptibility to oral cancer," in: *Journal of Oral Research* 4, 8-9. https://doi.org/10.17126/joralres.2015.003

Ruth, F., Soeratri, W., Hariyadi, D. M., El Muttaqien, S., Munfadlila, A. W., Sekaringtyas, F. C., and Rosyidah, A. (2025). "Gold nanoparticle synthesized from *Centella asiatica*: Emphasis on optimization, characterization, antioxidant, antiglycation, and cytotoxicity effect as an anti-aging cosmetic ingredient," *BioNanoScience* 15, 45. https://doi.org/10.1007/s12668-024-01713-5

Santhosh, P. B., Genova, J., and Chamati, H. (2022). "Green synthesis of gold nanoparticles: An eco-friendly approach," *Chemistry* 4, 345-369. https://doi.org/10.3390/chemistry4020026

Saravanan, M., Barabadi, H., and Vahidi, H. (2021). "Green nanotechnology: Isolation of bioactive molecules and modified approach of biosynthesis," in: *Biogenic Nanoparticles for Cancer Theranostics*, *Micro and Nano Technologies Series*. 101–122. https://doi.org/10.1016/C2019-0-02790-2

Sharma, O. P., Makkar, H. P. S., and Dawra, R. K. (2007). "A review of the hepatotoxic plant *Lantana camara*," *Crit. Rev. Toxicol.* 37, 313-352. https://doi.org/10.1080/10408440601177863

Simon, H. U., Haj-Yehia, A., and Levi-Schaffer, F. (2000). "Role of reactive oxygen species (ROS) in apoptosis induction," *Apoptosis* 5, article 415. https://doi.org/10.1023/A:1009616228304

Sujir, N., Ahmed, J., Pai, K.M., Denny, C., and Shenoy, N. (2019). "Challenges in early diagnosis of oral cancer: Case series," in: *Acta Stomatologica Croatica* 53 (2), 174-180. https://doi.org/10.15644/asc53/2/10

Sun, B., Hu, N., Han, L., Pi, Y., Gao, Y., Chen, K. (2019). "Anticancer activity of green-synthesized gold nanoparticles from *Marsdenia tenacissima* inhibits A549 cell proliferation through the apoptotic pathway," *Artif. Cells Nanomed. Biotechnol.* 47, 4012-4019. https://doi.org/10.1080/21691401.2019.1575844

Tayyeb, J. Z., Priya, M., Guru, A., Kishore Kumar, M.S., Giri, J., Garg, A., Agrawal, Rutvi., Mat, K. B., and Arockiaraj, J. (2024). "Multifunctional curcumin-mediated zinc oxide nanoparticles enhancing biofilm inhibition and targeting apoptotic pathways in oral squamous carcinoma cells," *Molecular Biology Reports* 51, article 423. https://doi.org/10.1007/s11033-024-09407-7

Warnakulasuriya, S. (2009). "Global epidemiology of oral and oropharyngeal cancer," *Oral Oncology* 45, 309-316. https://doi.org/10.1016/j.oraloncology.2008.06.002

Yao, Y., Zhou, Y., Liu, L., Liu, L., Xu, Y., Chen, Q., Wang ,Y., Wu, S., Deng, Y., Zhang, J., and Shao, A. (2020). "Nanoparticle-based drug delivery in cancer therapy and its role in overcoming drug resistance," *Frontiers in Molecular Biosciences* 7, article 193. https://doi.org/10.3389/fmolb.2020.00193

Article submitted: June 20, 2026; Peer review completed: July 19, 2026; Revised version received and accepted: August 10, 2026; Published: August 28, 2026.
DOI: 10.15376/biores.21.4.10205-10223